ISSN 1063-7710, Acoustical Physics, 2025, Vol. 71, No. 3, pp. 465–473. © Pleiades Publishing, Ltd., 2025.

ACOUSTICS OF LIVING SYSTEMS. BIOMEDICAL ACOUSTICS

Experimental Modeling of Imaging Artifacts in Ultrasound Examination of Human Lungs

S. D. Sorokin[a], *, M. V. Ryabkov[a], S. A. Tsysar[a], O. A. Sapozhnikov[a], and V. A. Khokhlova[a]

[a] *Moscow State University, Faculty of Physics, Moscow, 119991 Russia*

**e-mail: srknstepan@gmail.com*

Received July 25, 2024; revised February 14, 2025; accepted May 6, 2025

Abstract—To reveal the nature of artifacts in ultrasound images of human lungs (so-called B-lines), experimental phantoms were created consisting of a silicone layer for acoustic imitation of intercostal muscles, a layer formed with finely pored foam burn dressing imitating healthy or edematous lung tissue, a foam dressing fragment, a mandarin juice sac, and a drop of ultrasound gel imitating the structures of the lung tissue. Ultrasound (US) images were recorded with a linear ultrasonic probe L7-4 connected to a Verasonics V-1 scanner. Additionally, an image of a mandarin juice sac located on the surface of the water was constructed using the synthetic aperture method with an Olympus focused piezoelectric transducer. The resulting echograms were compared with images recorded in clinical cases of pulmonary pathologies. It is shown that the appearance of B-lines is associated with the effects of multiple reverberation in liquid-filled structures imitating lung tissue, while their brightness and width on the echogram depend on the characteristic size of the internal structure of the phantom.

Keywords: lungs, ultrasound diagnostics, artifacts of ultrasonic images, B-lines

DOI: 10.1134/S1063771024602413

1. INTRODUCTION

The need to treat pulmonary diseases and their complications has stimulated the development of methods for diagnostics and therapy of these pathological conditions [1]. Interest in such approaches has grown significantly in recent years, particularly during the SARS-CoV-2 pandemic. The most commonly used imaging modality for examining and identifying various pulmonary dysfunctions, including pneumonia, pneumothorax, fibrosis, and consolidation, is computed tomography (CT) [5, 6]. Ultrasound (US) examination offers an alternative, although the diagnostic capabilities of this method are limited, since the gas-saturated tissue of the lungs prevents US propagation. On the other hand, CT uses ionizing X-ray radiation, has a number of contraindications, and is inferior to US in terms of safety, cost, and mobility.

In US examination of pathological lung conditions, the primary source of information is the echographic image, characterized by multiple acoustic artifacts known as "comet-tails" or B-lines. The presence of these artifacts correlates with increased extravascular lung fluid and interstitial lung diseases, characterized by thickening of the interalveolar septa and often leading to pulmonary fibrosis [7, 8]. The characteristics and physical mechanisms of artifact formation are not yet fully understood [9].

Clinical cases can be broadly grouped by whether they affect the pleura or the internal lung structures, specifically the interstitium and alveoli. The manifestation of pleural pathologies on US images remains beyond the scope of this study, despite the fact they are also of significant scientific interest [10, 11].

Distinct vertical echogenic artifacts (B-lines) occur in conditions such as pulmonary edema and inflammatory processes in the lungs of various etiologies, contusions, acute respiratory distress syndrome (ARDS), and other diseases. These pathologies are accompanied by changes in the interstitial tissue of the lung, such as accumulation of extravascular fluid, thickening of interlobular septa, and development of fibrosis [12]. A higher number of B-lines that appear on the echogram correlates with more severe lung pathology [11]. According to the established diagnostic protocols, the presence of one or two B-lines in one intercostal space is usually considered normal. Three or more B-lines are interpreted as a sign of impaired lung aeration resulting from an increased volume of fluid of various origins and/or fibrous tissue within the interstitium relative to the air component [7, 13]. In cases of pronounced interstitial changes, filling of the interstitium with pathological fluid occurs in larger

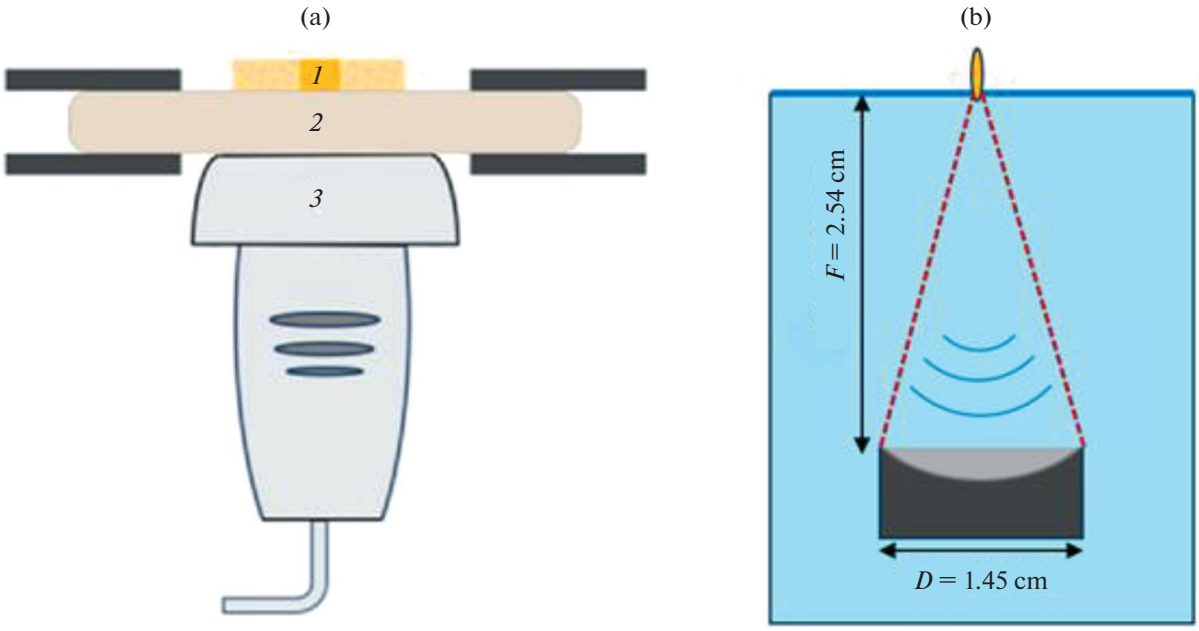

Fig. 1. (a) Schematic diagram of setup for observing image artifacts for different lung tissue phantoms: *1*, phantom; *2*, silicone layer; *3*, US L7-4 probe (ATL, Bothell, USA). (b) Schematic diagram of setup for recording a signal from piezoelectric transducer reflected from different points on the surface of water and a phantom of the edematous region of lungs in the form of mandarin juice sac. OlympusV307 US transducer was translated parallel to the water surface.

areas, which leads to a significant reduction in lung aeration; in this case, the US image changes to a continuous echogenic background behind the pleural line. This pattern, termed "white lung," has diagnostic power and indicates the presence of severe interstitial lung pathology, which may precede its consolidation [13, 14]. Acute respiratory distress syndrome (ARDS) in newborns, in severe cases of which the white lung artifact is observed, is a key example where US diagnostics is relevant as many other diagnostic modalities are not suitable [4].

The aim of this paper was to assess the possible physical mechanisms underlying the appearance of B-lines or comet-tail artifacts in US images, the formation of which is caused by the propagation and scattering of US waves in discretely aerated tissues of variable density. In a model experiment, the formation of echogenic artifacts was investigated on phantoms specially selected for their acoustic properties, simulating the structural elements of the lungs.

2. METHODS

2.1. Preparation of Phantoms and Experimental Setup with an Ultrasound Probe

During lung US imaging, an elastic wave passes through three tissue layers with different acoustic properties: the intercostal muscle, the pleural sac, and the lung tissue itself, which may exhibit varying degrees of fluid content [15, 16]. For this study, two-layer phantoms were created. The first layer, in the form of two-component silicone, imitated soft tissues; the second layer, in the form of a dry or wet finely pored foam burn dressing (sponge), a fragment thereof, a mandarin juice sac, or a drop of US gel, modeled different conditions of lung tissue.

The first layer was fabricated using two-component silicone (Elastosil-based Tool Decor 15, Germany). Liquid silicone and a platinum vulcanization catalyst were mixed in a smooth glass mold (11 × 11 cm) specially selected for the setup. After hardening, the silicone layer was removed from the mold, secured between metal plates (8 × 4 cm), and tightly clamped with a bolt. The following phantoms were then sequentially placed on the silicone layer: a dry or water-filled finely pored sponge; a sponge fragment on a layer of gel; two water drops covered with a sponge; a mandarin juice sac; a drop of US gel (Mediagel, Geltek-Medica, Moscow, Russia).

Two experimental setups were employed, the diagrams of which are shown in Fig. 1. Image artifacts for the different lung tissue phantoms were observed using first setup (Fig. 1a), consisting of a Verasonics V-1 US scanner (Redmond, USA), a stand with a clamp (not shown), an L7-4 US transducer (ATL, Bothell, USA), a silicone layer, and five different lung tissue phantoms.

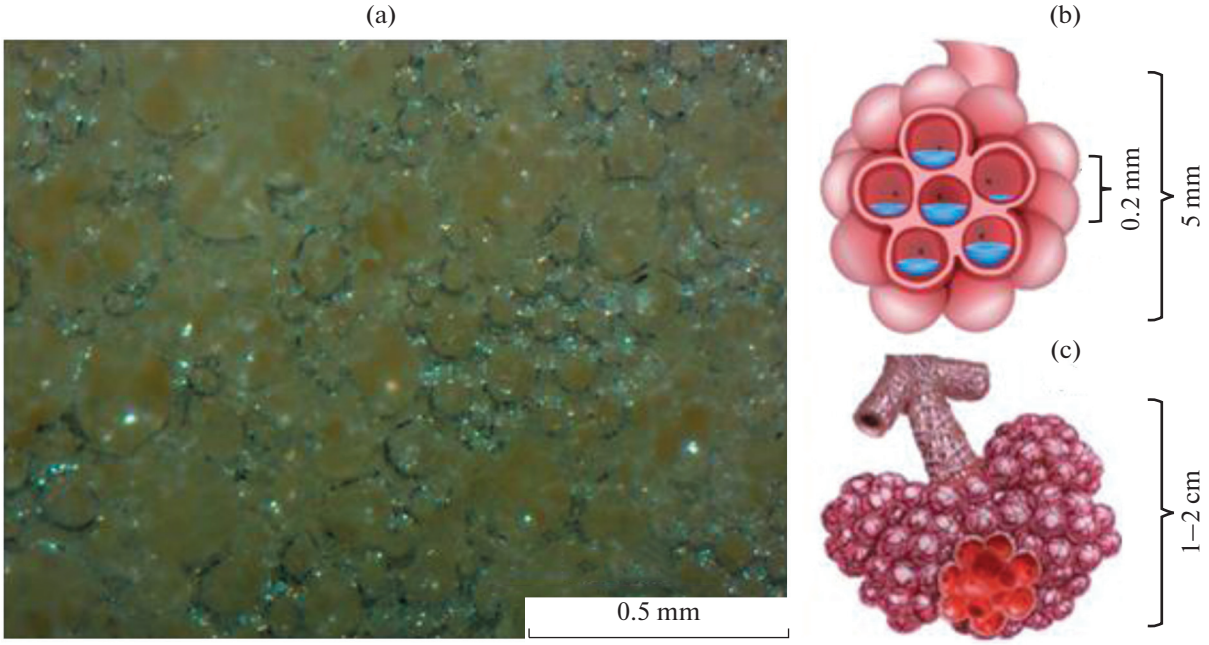

Fig. 2. (a) Photograph of dry finely pored sponge under a microscope (Stemi 2000 by Carl Zeiss, Germany). (b) Characteristic dimensions of sponge pores comparable to structural elements of human lungs, namely, alveoli (0.2 mm); characteristic size of a juice sac of mandarin (3 × 5 mm) corresponds to the dimensions of acinus. (c) Fragment of the wet sponge and drop of US gel are commensurate with lung lobe (1–2 cm).

Using a stereomicroscope (Stemi 2000, Carl Zeiss, Germany), a photograph of a finely pored sponge was taken (Fig. 2a), in which its structure and pore sizes are clearly visible. This image demonstrates the correspondence between the characteristic sizes of the sponge pores and the pulmonary alveoli (~0.2 mm), indicating an appropriate model choice with similarity to real lung tissue (Fig. 2b) [17, 18]. Similarly, the characteristic size of the mandarin juice sac (3 × 5 mm) is comparable to the size of a lung acinus (Fig. 2b). A fragment of the wet sponge and a drop of US gel can be compared with a lung lobe (typical size 1–2 cm, Fig. 2c).

The first step in preparing the two-layer samples involved creating the silicone layer, whose thickness and homogeneity were crucial. Subsequently, the second layer was prepared using pre-selected phantoms; their characteristic dimensions were measured and adjusted. For phantoms involving wet sponge, it was pre-soaked and then wrung out underwater to minimize air content in the pores. The setup was assembled, the ATL L7-4 US probe (Philips, Bothell, USA) with US gel applied to its surface was connected to the Verasonics V-1 US scanner, and the scanning was performed. Most echograms were acquired using the finely pored sponge phantom (Fig. 3a) in three states: dry, completely water-filled, and after absorbing two water drops from the silicone surface. A subsequent series of measurements was carried out with three smaller phantoms: a wet fragment of the sponge, a mandarin juice sac, and a drop of US gel (Fig. 3b–3d). Each phantom was placed sequentially on a silicone layer for image recording with the linear US probe, as shown in Fig. 1a. To ensure acoustic contact and hold the phantoms in a vertical position, their lower end was lubricated with a small amount of US gel.

2.2. Experiment with a Single-Element Focused Piezoelectric Transducer

A single-element focusing US transducer was used to quantitatively analyze the temporal shape of signals reflected from the phantoms. The Olympus V307 transducer was used having a diameter of 14.5 mm and a focal length of 25.4 mm (Waltham, USA), which has the same frequency band as the L7-4 linear probe (4–7 MHz at the –6 dB level). This transducer operated in single-channel mode for both emission and reception. Hydrophone measurements of the generated signal profiles were carried out to verify the similarity of acoustic pulses emitted by the linear multi-element US probe and the single-element focusing piezoelectric transducer.

The capsule hydrophone HGL-0200 (Onda, UK) and the L7-4 probe were placed facing each other in a water tank. The hydrophone was attached to a

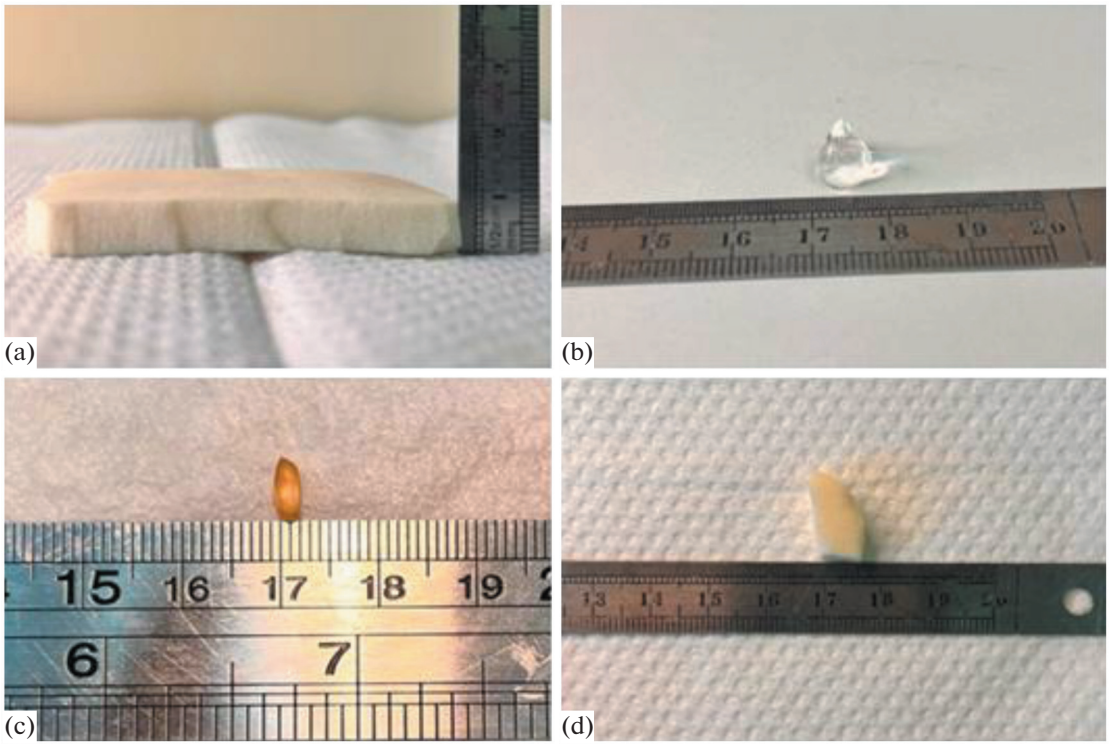

Fig. 3. Photographs of phantoms used in the experiment: (a) finely pored burn foam dressing (sponge) (thickness—8 mm); (b) wet sponge fragment (7mm × 10 mm); (c) mandarin juice sac (3 mm × 5 mm); (d) drop of US gel (6 mm × 7 mm)

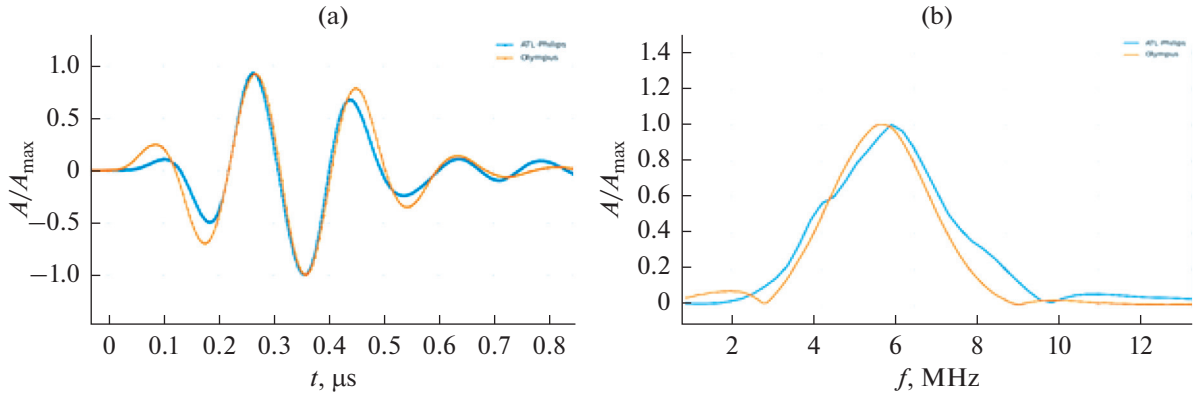

Fig. 4. (a) Comparison of temporal waveforms and (b) spectra of pulse signals of the L7-4 US probe (blue curve) and single-element piezoelectric transducer Olympus V307 (orange curve).

mechanical positioning system, while the ultrasonic probe was fixed on a static tripod. Measurements of the hydrophone electrical signal profiles as a function of time were performed at two different distances (15 and 50 mm). The US probe was then replaced with the Olympus V307 transducer and the hydrophone signal was recorded at the transducer's focal point. By adjusting the frequency of the generator's signal and the number of cycles, the hydrophone signal was made similar to the signal measured using the L7-4 ultrasonic probe as the source. As shown in Fig. 4, the signals were indeed nearly identical. This made it possible to study the effect of the phantom (a mandarin juice sac) on the shape of the reflected signal of the focusing source, and then to apply the synthetic aperture method to construct an US image of the specified phantom (see below).

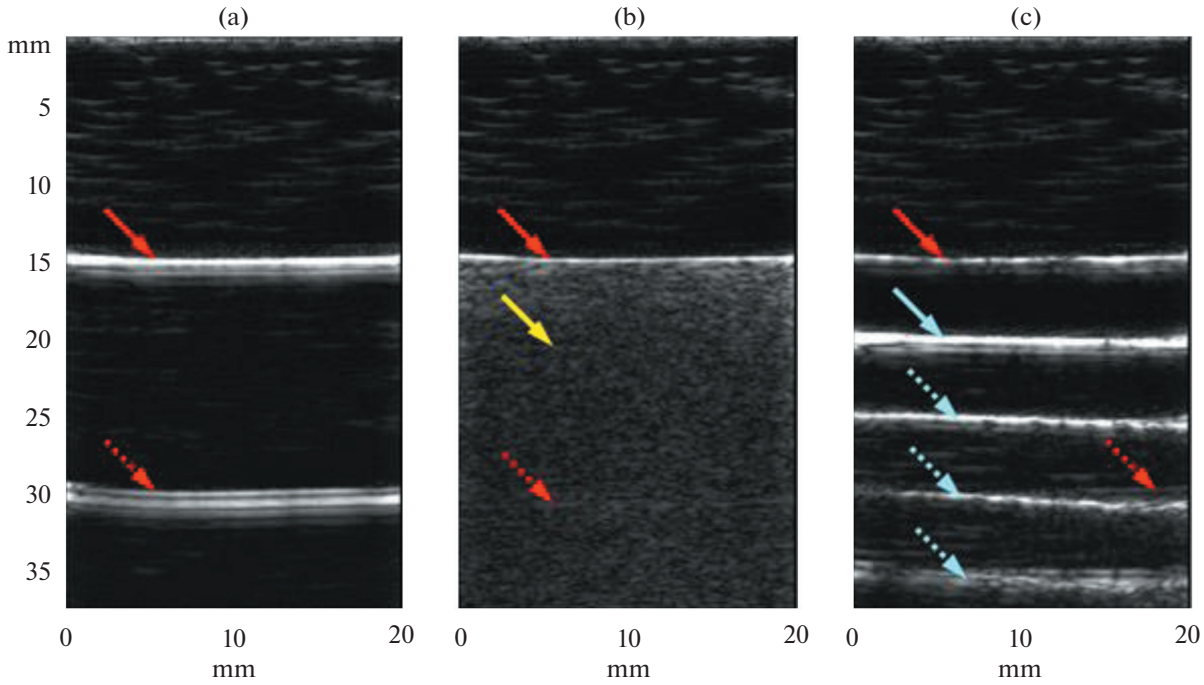

Fig. 5. US images obtained in B-mode (US L7-4 probe is located on top) through a silicone layer: (a) completely dry finely pored sponge; (b) completely wet sponge; (c) layer of water, thickness of which is equal to the thickness of sponge (8 mm). Solid red arrow marks echogenic line corresponding to reflection from boundary of silicone layer with sponge; dashed red arrow marks first reflection in the indicated layer. Yellow arrow indicates weak reflection from the back edge of fully wet sponge (b). Blue solid arrow corresponds to water–air boundary, and blue dashed arrows mark multiple reflections in the water layer (c).

2.3. Construction of an US Image Using Aperture Synthesis

The Olympus V307 transducer was placed in the tank at the focal distance from the water surface (Fig. 1b) and moved using an UMS-3 CNC positioning system (Precision Acoustics, UK). The mandarin juice sac was fixed vertically above the surface of the water, with its lower part touching the surface to form a meniscus. In this way, an edematous area of the lung was simulated, in contact with the adjacent soft tissues of the pleura, which conduct US. Acoustic pulses emitted by the transducer from different positions were reflected either from the water–air boundary or from the surface of the mandarin juice sac/air interface and received by the same transducer. The transducer was moved, and echo signals were measured in a plane parallel to the water surface with a step of 0.2 mm. Before forming the B-scan, signals were prefiltered in the frequency band from 0.1 to 20 MHz using a Blackman–Harris window to suppress external noise [19]. The signal envelope was constructed using the Hilbert transform [20]. Combining the obtained linear (vertical) profiles of echo signals based on their peak values, a two-dimensional image was constructed, along the central line of which a B-scan was formed, similar to that obtained using an US scanner with the L7-4 linear probe.

3. RESULTS

3.1. Artifacts of US Images of Phantoms

Using the medical L7-4 linear probe (Fig. 1a), echograms of various phantoms were obtained, which showed artifacts analogous to B-lines observed in pulmonary pathologies.

Figure 5 shows US scans of the first series of echograms, illustrating the differences between the images of a completely dry sponge simulating healthy lung tissue, a completely wet sponge simulating severe pulmonary edema, and a layer of water with the same thickness as the sponge. In the images, the probe is on top, the distance is measured from the probe down. The spatial coordinates of the original image were scaled so that the thickness of the silicone layer corresponded to the true one (15 mm). In this case, a water layer of 8 mm thickness is visible in the image as a layer of 5 mm thickness due to the difference in the sound speed in silicone and water.

As Fig. 5a shows, for the dry sponge, a total signal reflection occurred at the silicone-sponge boundary, appearing as a bright echogenic horizontal line at

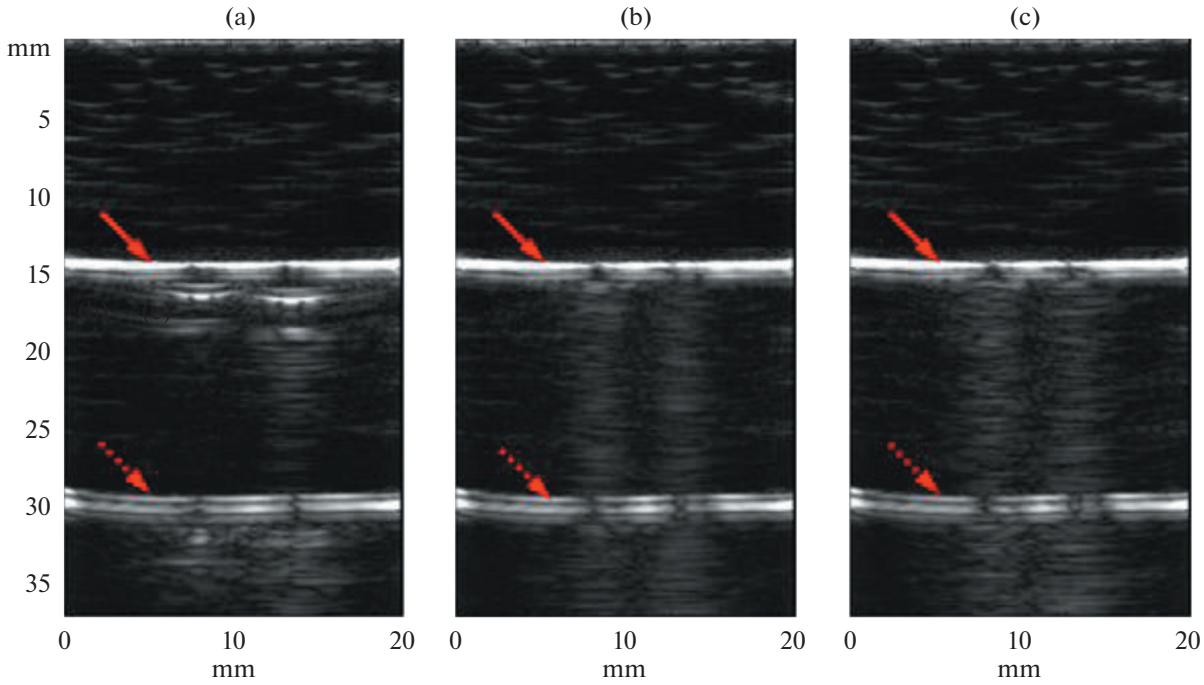

Fig. 6. B-lines on US images: (a) two drops of water on the silicone layer without sponge; (b) immediately after sorption of drops by dry sponge; (c) after 60 s of placing the sponge on the drops. US probe is located on top. Solid red arrow marks echogenic band corresponding to the reflection from the boundary of silicone layer with sponge; dashed red arrow marks first reflection in the indicated layer.

15mm distance from the probe (red solid arrow). In this case, the image of the dry sponge is absolutely dark; its boundary distant from the probe is not visible, but an artifact is visible in the image as an echogenic line 30 mm from the probe, corresponding to the first reflection of the signal in the silicone layer (red dashed arrow).

The image of the wet sponge (Fig. 5b) showed a bright echogenic region beyond the silicon boundary with contrast decreasing with depth. The boundary line between the silicone and the wet sponge (solid red arrow) is less bright compared to the case of a dry sponge (Fig. 5a), since there is no total reflection of the acoustic signal. The sponge's distant boundary (yellow arrow) and the artifact of the repeated silicone boundary (red dashed arrow) are barely noticeable in the image, which indicates significant US penetration through the silicone–sponge boundary. Ultrasound pulse is repeatedly scattered inside the sponge, almost not reaching its far boundary, and returns to the probe through the near boundary of the sponge with increasing delays. Thus, a wet sponge is a strong scatterer, but US penetrates to some depth and is scattered many times, instead of being reflected from the boundary with silicone as in the case of a dry sponge.

Figure 5c shows an image of the water layer on silicone with the same thickness as the sponge (8 mm). Although water and the wet sponge have similar impedances and US penetrates well in both cases through the boundary with silicone, no scatterers are present in water, which results in significantly different image. On the echogram with the water layer, the solid red arrow marks its boundary with silicone, the solid blue arrow marks the brightest line corresponding to the reflection of the US signal from the boundary with air at a distance of 20 mm from the probe. Three repeated bright bands are visible at distances of 25, 30 and 35 mm, arising due to multiple reflections in the water layer between its boundaries with silicone and air. A weak echogenic artifact of reflection in the silicone layer may also be present at a distance of 30 mm from the probe (red dashed arrow).

The second series of echograms (Fig. 6) was obtained by placing two drops of water on the silicone surface and as a result of their absorption by a dry finely pored sponge. Without the sponge, due to reflections inside of free water drops, an acoustic trap arises in each of them, forming B-lines with a non-uniform structure (Fig. 6a). At the initial section of the lines, two bright horizontal stripes are visible, corresponding to reflections between the rear surface of the drop and its boundary with the silicone. After placing the sponge on the drops, the structure of the B-lines becomes different (Fig. 6b, 6c). As water penetrates

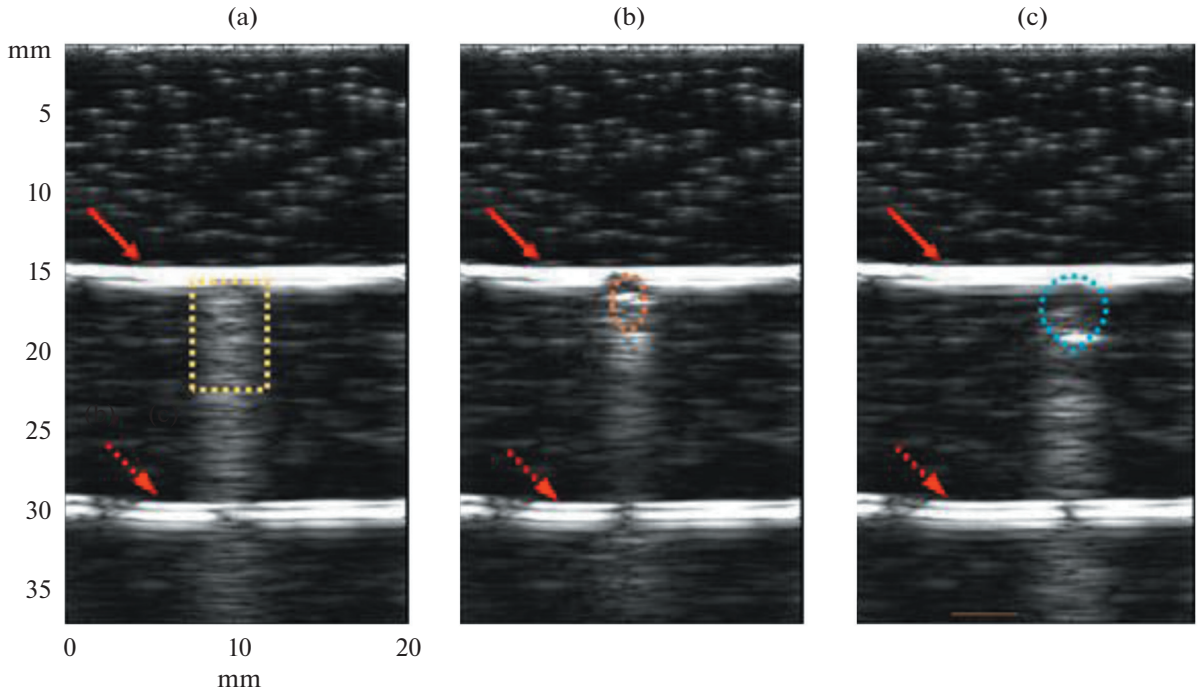

Fig. 7. US images of lung tissue phantoms located on surface of a silicone layer (Fig. 1a): (a) fragment of wet sponge; (b) mandarin juice sac; (c) drops of US gel. US probe is located on top. Solid red arrow marks echogenic line corresponding to the reflection from the boundary of the silicone layer with sponge; dashed red arrow indicates first reflection in indicated layer. Dotted contours illustrate characteristic geometric contours and dimensions of the phantoms.

the pores of the sponge, the shape, size, and structure of the acoustic trap gradually change. Multiple scattering within the water-filled sponge pores led to ultrasonic waves escaping from the sponge to the probe with increasing delays, forming B-lines with a more uniform structure. As the comparison of the length of the echogenic lines in Fig. 6a and 6b shows, acoustic waves are retained in free drops (Fig. 6a) for shorter time than in a sponge that has absorbed these drops (sponge with "edema"). In turn, some broadening of the B-lines in Fig. 6c compared to Fig. 6b can be explained by the diffusion of water through the pores of the sponge over time, which leads to expansion of the "swelling" area.

The third series of similar echograms was obtained for three phantoms simulating individual structural elements of the lungs (Fig. 3): a wet fragment of a finely pored sponge (7 × 10 mm), the mandarin juice sac, and a drop of US gel. The echograms shown in Fig. 7 illustrate typical single artifacts in the form of B-lines, which confirms the previous assumptions about the correspondence of the selected phantoms to pathological lung tissue in terms of acoustic properties. The spatial coordinates of the initial image, like in Fig. 5, 6, are scaled so that the thickness of the silicone layer corresponds to the true one (15 mm). Dotted contours illustrate the approximate geometric contours and dimensions of the phantoms, assuming that the sound speed in phantoms is equal to that in water.

3.2. Artifacts of US Images Constructed Using the Synthetic Aperture Method

To exclude the possibility of the influence of the method of imaging construction by the diagnostic US system, which can introduce additional artifacts, the following imaging experiment was conducted using the aperture synthesis method. Figure 1b shows a diagram of the setup. The aim of this experiment was to observe B-line artifacts in imaging echoes from the mandarin juice sac placed on the water surface. For the measurements, an Olympus V307 ultrasonic piezoelectric transducer was used, the signal of which was similar to that generated by the Phillips ATL L7-4 linear probe (Fig. 4).

Figure 8 shows the results of measuring echo signals, filtering them, and constructing a two-dimensional image of a tissue phantom on the water surface. Using the synthetic aperture method, a rectangular area of the water surface was scanned using a positioning system. A distribution of peak envelope values was obtained by processing a set of linear signal profiles (Fig. 8a,b), in the center of which is a meniscus formed by the juice sac of the mandarin. By selecting

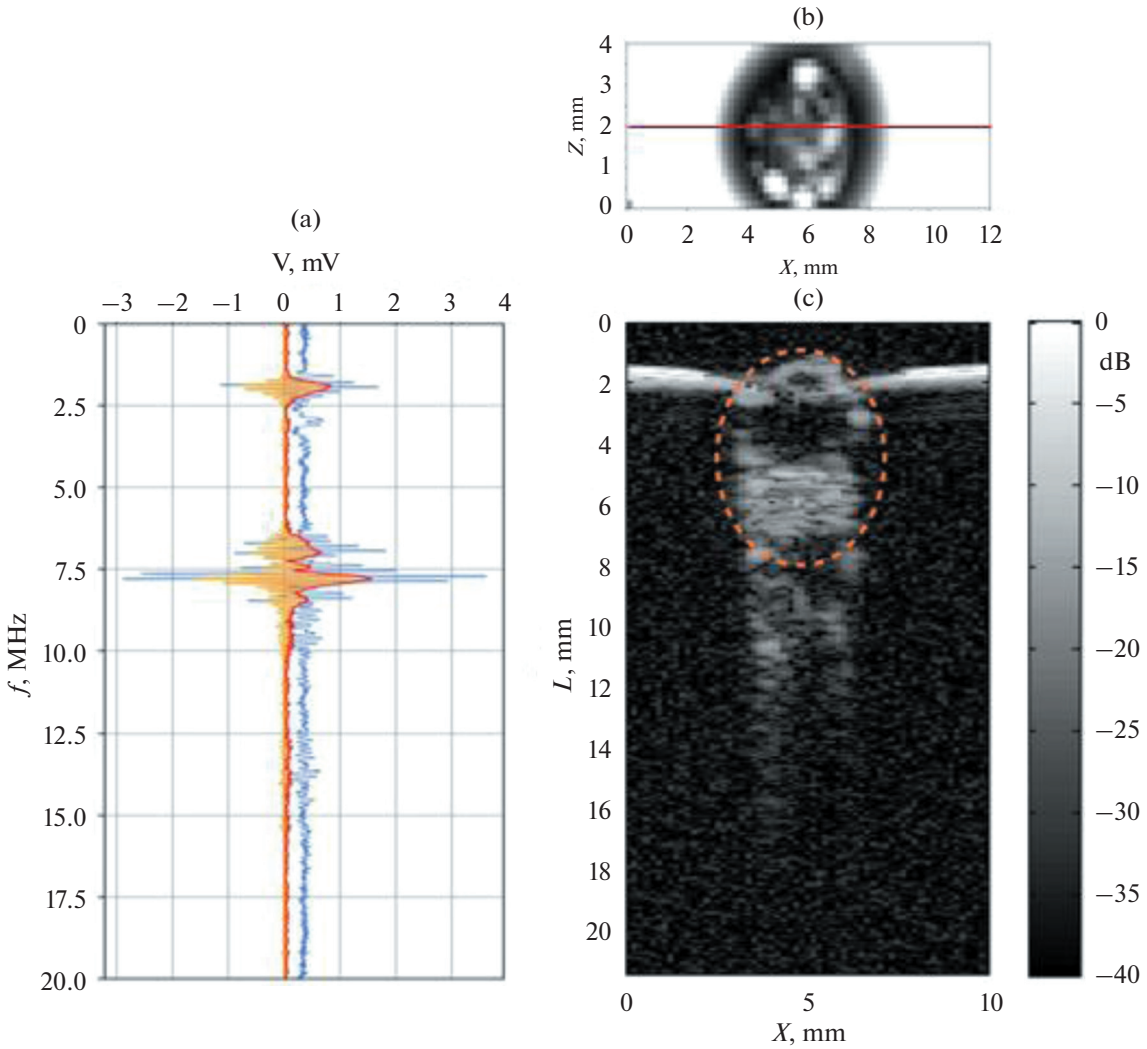

Fig. 8. (a) RAW (blue) original signal, filtered (mandarin) signal after filtering with Blackman–Harris window from 0.1 to 20 MHz, envelope (red) of signal obtained using the Hilbert transform after zero-frequency rejection. (b) Rectangular scan of mandarin juice sac on the water surface. Red line marks section on plane along which the image of juice sac was constructed in B-mode. (c) B-scan, where orange dashed outline corresponds to the shape, size, and location of juice sac.

a plane for the B-scan that passes through the center of the phantom (marked with a red line in Fig. 8b), one can observe an image (Fig. 8c) like the US image obtained in B-mode using a diagnostic US system. The timeline t of echo signal delays was recalculated in the figure into the corresponding distance $z = ct/2$, where $c = 1480$ m/s is the sound speed in water and $z = 0$ corresponds to the distance of 2 mm above the water surface. An artifact similar to the one present in Fig. 6b is distinguished, confirming that the mechanism underlying the appearance of the B-line in this case is caused not by processing the probe signal by the diagnostic US system, but by the physical process of reverberation of the acoustic pulse inside the phantom and the corresponding delays in the output and broadening of the echo signal.

4. CONCLUSIONS

This study employed two experimental arrangements to simulate US imaging artifacts typical for pulmonary diseases. The characteristic dimensions of the structural elements of the phantoms selected for modeling were assessed. It was shown that on phantoms of lung tissue with edemas in the form of a fragment of a finely pored sponge of foam burn dressing, a mandarin juice sac, and a drop of US gel, US artifacts are observed that are identical to vertical echogenic artifacts that occur in various pathological conditions of the lungs. A qualitative explanation is proposed for the correlation between the obtained US images and artifacts occurring in medical research. To confirm the physical mechanism of the resulting B-line artifacts, images of the mandarin juice sac on the water surface

were constructed by the synthetic aperture method with a single-element Olympus V307 transducer, which was used both as a source and as a receiver. Images were obtained containing B-line artifacts similar to those recorded with a US scanner on various phantoms.

The experiments conducted in this study on simple phantoms simulating lung tissue illustrate the hypothesis that the mechanism for the occurrence of a B-line artifact is the trapping and reverberation of an ultrasonic pulse inside an acoustic trap. Although the general concept and physical mechanism of the acoustic trap have been recognized and are commonly used in interpreting the occurrence of B-line artifacts, a complete understanding of the correspondence of various pathological conditions of the lung to trap models with specific parameters has not yet been reached. The experiments examined and compared several simple models of B-line formation in the lungs, which can be attributed to different etiologies. It is analyzed which manifestations of B-lines they model and how they differ. Such a comparison has not been made before. In the future, with further development, such models with well-controlled acoustic properties can be used both for educational purposes and for the development of specific modalities of US diagnostics of pulmonary diseases.

The direct measurements of US echo signals and the US image constructed on their basis also illustrate new possibilities for analyzing emerging artifacts and correlating them with various diseases. For example, changes in these signals due to altered acoustic properties of lung tissue could be used to monitor the condition of patients [2]. Detection and quantitative study of features of "raw" acoustic signals would allow advances in interpreting the obtained images, understanding the observed artifacts, developing new methods for diagnosing patients with pulmonary pathologies, and creating new devices specially designed for lung sonography.

ACKNOWLEDGMENTS

The authors thank A.V. Kadrev for useful discussions.

FUNDING

The research was carried out under the state assignment of Moscow State University and with the support of the student scholarship of the Foundation for the Development of Theoretical Physics and Mathematics "BASIS" 23-2-1-44-1.

CONFLICT OF INTEREST

The authors of this work declare that they have no conflicts of interest.

REFERENCES

1. A. P. Makarenkov and A. G. Rudnitskii, Acoust. Phys. **41** (2), 234 (1995).
2. T. D. Khokhlova, G. P. Thomas, J. Hall, K. Steinbock, J. Thiel, B. W. Cunitz, M. R. Bailey, L. Anderson, R. Kessler, M. K. Hall, et al., J. Ultrasound Med. **43** (3), 513 (2024).
3. S. Mika, W. Gola, M. Gil-Mika, M. Wilk, and H. Misiołek, *Anaesthesiol. Intensive Ther.* **56** (1), 1 (2024).
4. F. Mento and L. Demi, J. Acoust. Soc. Am. **150** (6), 4075 (2021).
5. S. Raju, S. Ghosh, and A. C. Mehta, Chest **151** (6), 1356 (2017).
6. J. F. Gruden, D. P. Naidich, S. C. Machnicki, S. L. Cohen, F. Girvin, and S. Raoof, Chest **157** (3), 612 (2020).
7. G. Volpicelli, Chest **158** (4), 1323 (2020).
8. V. Berce, M. Tomazin, M. Gorenjak, T. Berce, and B. Lovrenčič, Sci. Rep. **9** (1), 17957 (2019).
9. M. Di Serafino, M. Notaro, G. Rea, F. Iacobellis, V. D. Paoli, C. Acampora, S. Ianniello, L. Brunese, L. Romano, and G. Vallone, Radiol. Med. **125**, 738 (2020).
10. D. Lichtenstein, Chest **147** (6), 1659 (2015).
11. V. V. Mit'kov, D. V. Safonov, M. D. Mit'kova, M. N. Alekhin, A. N. Katrich, Yu. V. Kabin, N. N. Vetsheva, E. D. Khudorozhkova, R. E. Lakhin, A. V. Kadrev, et al., Ul'trazvukovaya Funkts. Diagn. **1**, 46 (2020).
12. D. Lichtenstein, G. Mézière, P. Biderman, A. Gepner, and O. Barré, Am. J. Respir. Crit. Care Med. **156** (5), 1640 (1997).
13. G. Soldati, A. Smargiassi, L. Demi, and R. Inchingolo, Appl. Sci. **10** (5), 1570 (2020).
14. M. Demi, R. Prediletto, G. Soldati, and L. Demi, IEEE Trans. Ultrason. Ferroelectr. Freq. Control **67** (3), 612 (2020).
15. T. Kameda, N. Kamiyama, H. Kobayashi, Y. Kanayama, and N. Taniguchi, Ultrasound Med. Biol. **45** (7), 1617 (2019).
16. G. Soldati, V. Giunta, S. Sher, F. Melosi, and C. Dini, Ultrasound Med. Biol. **37** (11), 1762 (2011).
17. D. M. Hansell, A. A. Bankier, MacMahon, H., McLoud, T.C., Müller, N.L., and Remy, J., Radiology **246** (3), 697 (2008).
18. D. M. Hyde, N. K. Tyler, L. F. Putney, P. Singh, and H. J. Gundersen, Anat. Rec. A **277** (1), 216 (2004).
19. Q. Jingwen, G. Maofa, and W. Xiaoyu, Appl. Mech. Mater. **330**, 977 (2013).
20. S. O. Sadjadi, T. Hasan, and J. H. L. Hansen, in *Proc. 13th Annual Conf. of the Int. Speech Communication Association 2012, INTERSPEECH 2012* (Portland, OR, 2012), Vol. 2, p. 1694.

Publisher's Note. Pleiades Publishing remains neutral with regard to jurisdictional claims in published maps and institutional affiliations.
AI tools may have been used in the translation or editing of this article.

SPELL: 1. OK